Structural stability of NiCoFeCrAl$_x$ high-entropy alloy from *ab initio* theory

Fuyang Tian,[1,2] Lorand Delczeg,[1] Nanxian Chen,[2,3] Lajos Karoly Varga,[4] Jiang Shen,[2] and Levente Vitos[1,4,5]

[1]*Applied Materials Physics, Department of Materials Science and Engineering, Royal Institute of Technology, Stockholm SE-100 44, Sweden*

[2]*Institute for Applied Physics, University of Science and Technology Beijing, Beijing 100083, China*

[3]*Department of Physics, Tsinghua University, Beijing 100084, China*

[4]*Wigner Research Centre for Physics, Institute for Solid State Physics and Optics, H-1525 Budapest, P.O. Box 49, Hungary*

[5]*Department of Physics and Astronomy, Division of Materials Theory, Uppsala University, Box 516, SE-751210, Uppsala, Sweden*

(Received 2 April 2013; published 30 August 2013)

First-principles alloy theory predicts that at room temperature the paramagnetic NiCoFeCrAl$_x$ high entropy alloys adopt the face centered cubic (fcc) structure for $x \lesssim 0.60$ and the body centered cubic (bcc) structure for $x \gtrsim 1.23$, with an fcc-bcc duplex region in between the two pure phases. The calculated single- and polycrystal elastic parameters exhibit strong composition and crystal structure dependence. Based on the present theoretical findings, it is concluded that alloys around the equimolar NiCoFeCrAl composition have superior mechanical performance as compared to the single-phase regions.

DOI: 10.1103/PhysRevB.88.085128 PACS number(s): 62.20.D−, 71.20.Be, 81.05.Bx

Due to the unique microstructure and special properties, such as high strength, good wear, corrosion resistance, and thermophysical parameters, high entropy alloys (HEAs) have attracted increasing attention since the pioneering works by Yeh *et al.*[1] In this promising new class of engineering materials, the high mixing entropy is responsible for the stability of the simple solid solution phases rather than a mixture of ordered intermetallic compounds.

Extensive experimental studies focused on the NiCoFeCrAl$_x$ system with $x = 0.0$–3.0.[2–13] The microstructure, mechanical, electronic, magnetic, and Hall properties were investigated for the as-cast, as-homogenized, and as-deformed NiCoFeCrAl$_x$ ($x = 0.0$–2.0) alloys.[2,3] With increasing Al content, the microstructure of NiCoFeCrAl$_x$ transforms from single fcc to single bcc with a transition duplex fcc/bcc region.[2,4] Zhou *et al.* used the vacuum arc melting method to prepare single phase bcc NiCoFeCrAl.[5,6] On the other hand, Chou *et al.* employing an arc remelter found that the microstructure of NiCoFeCrAl is a mixture of fcc and bcc phases.[4] Kao *et al.* further compared different experimental treatment and obtained the beginning of a single bcc phase at $x = 0.88$ for as-cast, and $x = 1.17$ for as-homogenized and as-deformed NiCoFeCrAl$_x$.[2] More recent results indicate that the microstructure of NiCoFeCrAl$_x$ is fcc for $x \leqslant 0.5$, fcc/bcc duplex for $0.5 < x < 0.9$, and bcc for $x \geqslant 0.9$.[10] Computational thermodynamic assessment of the phase diagram of NiCoFeCr-Al predicted that Al stabilizes the bcc structure.[13]

The average valence electron concentration (VEC) has been suggested to correlate well with the phase stability of HEAs.[14] In particular, equimolar NiCoFeCr, CuNiCoFeCr, NiCoFeMnCr, and PdNiCoFeCr have VEC $\geqslant 7.8$ and adopt pure fcc structure,[1,15,16] whereas equimolar NiCoFeCrTiAl has VEC $= 6.7$ and forms a single phase bcc solid solution.[5] Going beyond the empirical correlations, Zhou *et al.* used classic homogeneous nucleation theory[17] to explain the phase stability of CuNiCoFeCr and the phase transformation from fcc $Cu_{0.5}NiFeCrAl_{0.5}$ to bcc $Cu_{0.25}NiFeCrAl_{0.75}$. Here we move towards the atomic-level description of the interactions within the HEAs by adopting state-of-the-art *ab initio* density functional theory[18] to study the phase stability and the micromechanical properties of NiCoFeCrAl$_x$ as a function of Al content.

The exact muffin-tin orbitals (EMTO) method,[19–22] in combination with the coherent potential approximation (CPA),[23,24] was previously used to study the structural and mechanical properties of CuNiCoFeCr and CuNiCoFeCrTi$_x$ ($x = 0.1$–$0.5, 1.0$) HEAs.[25] In the present application, the EMTO equations were solved within the scalar-relativistic approximation using the Perdew-Burke-Ernzerhof exchange-correlation density functional.[26] The Green's function was calculated for 24 complex energy points around the valence states. The basis set included s, p, d, and f states. The irreducible wedge of the fcc (bcc) Brillouin zone was sampled by 240 (285) inequivalent k points. The electrostatic correction to the single-site CPA was described using the screened impurity model[27] with screening parameter 0.6. All calculations were performed for static lattice. The equilibrium volume, bulk modulus, and total energy were extracted from a Morse function[28] fitted to the total energies calculated for seven different volumes. The singe-crystal elastic constants were determined according to the standard methodology and the polycrystal elastic moduli were obtained via the Voigt-Reuss-Hill averaging method.[29]

The magnetic properties of NiCoFeCrAl$_x$ ($0 \leqslant x \leqslant 2.0$) were investigated by several authors.[3,4,15] According to the recent magnetization measurements by Lucas *et al.*,[15] NiCoFeCr is paramagnetic at room temperature and $NiCoFeCrAl_2$ has Curie temperature around 430 ± 3 K. The estimated critical temperatures by Kao *et al.*[3] range between 120 K ($x = 0$) and 375 K ($x = 2$), in good agreement with those reported by Lucas *et al.* Considering that these transition temperatures are relatively low, here we assume a paramagnetic (PM) state for all NiCoFeCrAl$_x$ alloys. We describe the PM state by the disordered local magnetic moment (DLM) picture.[30] The DLM was shown to correctly account for the random distribution of the local magnetic moments of the PM state of metals well above the magnetic transition temperature, where the magnetic moments show negligible short range order.[31–33] For fcc NiCoFeCrAl$_x$, we find that the local magnetic moment of Fe increases from 1.79 to 1.96 μ_B as going from $x = 0$

TABLE I. Theoretical Wigner-Seitz radius (w, units of Bohr), bulk modulus (B, units of GPa), and energy difference between the bcc and fcc phases (ΔE_t, units of mRy per atom) for $NiCoFeCrAl_x$ high entropy alloys calculated for the fcc and bcc phases as a function of Al fraction x.

x	w(fcc)	B(fcc)	w(bcc)	B(bcc)	ΔE_t	x	w(fcc)	B(fcc)	w(bcc)	B(bcc)	ΔE_t
0	2.607	207	2.626	199	3.937	1.00	2.654	183	2.659	178	0.228
0.10	2.611	200	2.629	197	3.408	1.25	2.664	173	2.667	171	−0.236
0.25	2.619	197	2.634	193	2.523	1.30	2.666	172	2.670	170	−0.239
0.30	2.622	196	2.636	192	2.380	1.50	2.673	170	2.675	167	−0.449
0.375	2.626	194	2.639	189	2.021	2.00	2.691	159	2.690	159	−0.773
0.50	2.632	190	2.644	187	1.566	2.50	2.705	151	2.701	153	−0.831

to $x = 2$. For bcc $NiCoFeCrAl_x$, the Fe (Co) local magnetic moment changes from 2.29 μ_B (1.13 μ_B) to 2.08 μ_B (0.63 μ_B) when the Al content is increased from $x = 0$ to $x = 2$. All other local (DLM-level) magnetic moments are zero.

In Table I and the lower panel of Fig. 1 we show the theoretical Wigner-Seitz radius (w), equilibrium volume (V), bulk modulus (B), and structural energy difference $\Delta E_t \equiv E_t^{bcc} - E_t^{fcc}$ for the $NiCoFeCrAl_x$ alloys as a function of Al content. The theoretical equilibrium volumes of the fcc and bcc alloys are compared to the experimental data in the upper panels of Fig. 1. Experimental volumes are available for the single fcc phase for $x \leqslant 0.5$, and for single bcc phase for $x \geqslant 0.9$.[2,4,8,10] Taking into account the large scatter in the experimental data, we conclude that the present theory reproduces well the experimental trends of $V(x)$ for both fcc and bcc structures. Aluminum addition is found to increase the equilibrium volume of the solid solution, which is consistent with the fact that w of Al is larger than those of the other alloy components. The slopes of $w(x)$ and $B(x)$ versus x are larger in the fcc phase than in the bcc phase. This is likely to be due to the enhanced flexibility of the bcc structure to incorporate a large substitutional element as compared to the close-packed fcc lattice.

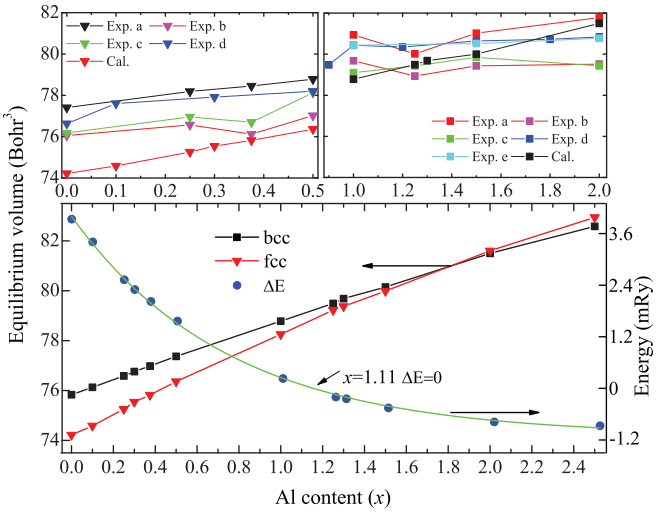

FIG. 1. (Color online) Upper panels: Comparison between the theoretic and experimental equilibrium volumes for fcc (x = 0.0–0.5, upper left panel) and bcc (x = 1.0–2.0, upper right panel) $FeCrNiCoAl_x$ alloys. The quoted experimental data are a Ref. 4, b and c Ref. 2, d Ref. 10, and e Ref. 8. Lower panel: Theoretical fcc and bcc equilibrium volumes and structural energy difference for $0 \leqslant x \leqslant 2.5$.

In order to assess the performance of our calculations derived from the mean-field CPA, we constructed two $2 \times 2 \times 2$ cubic supercells. The supercell formed by the bcc (fcc) unit cells was treated as simple cubic (body centered cubic), where we introduced one (two) Al atom per 16 (32) atomic sites. All other sites were occupied by an equimolar four component NiCoFeCr alloy. We note that similar partially ordered solid solution has been reported in $FeCrNiCoAl_{0.3}$ alloys.[7] The present supercells have the molar radio $Ni_{15/4}Co_{15/4}Fe_{15/4}Cr_{15/4}Al_1$, corresponding to $NiCoFeCrAl_{0.2667}$ HEA. The Wigner-Seitz radii obtained for these supercells are 2.620 Bohr for fcc, and 2.634 Bohr for bcc, which are practically the same as those obtained in the CPA calculations (2.620 Bohr for fcc and 2.635 for bcc). The corresponding bulk moduli are 197 and 193 GPa for the fcc and bcc supercells, respectively, which are also close to the CPA results (198 GPa for fcc and 193 GPa for bcc).

According to Table I, the fcc structure is predicted to be more stable than the bcc one for x = 0.0–1.0, and the bcc structure becomes stable from $x = 1.25$. Using a cubic spline fit for the calculated energy points, we find that the structural energy difference between ideal bcc and fcc lattices vanishes at 1.11 Al fraction (Fig. 1, lower panel). Due to the large atomic volume of Al, one may anticipate that the interatomic distance between Al and the other elements is larger than the average bulk value. We estimated the size of the local lattice relaxation (LLR) around the Al atoms in $NiCoFeCrAl_x$ alloys by making use of the above $2 \times 2 \times 2$ supercells, each of them containing one single Al atom. We relaxed the first 12 nearest neighbor NiCoFeCr sites in the fcc supercell and the first 8 nearest neighbor NiCoFeCr sites in the bcc supercell. For the energy gain upon the LLR, we obtained $\delta E_{bcc} = 0.17$ mRy and $\delta E_{fcc} = 0.32$ mRy. The larger relaxation effect in the fcc lattice is in line with our previous observation that the bcc lattice can accommodate the large substitutional Al easier than the fcc lattice. Then we consider $\Delta E_t^r \equiv x(\delta E_{bcc} - \delta E_{fcc})$ as the measure of the LLR effect on the structural energy difference per Al fraction. Adding ΔE_t^r to ΔE_t from Table I, we obtain that the total structural energy difference vanishes around $x = 1.2$, i.e., at only slightly larger Al content than the one predicted from the total energies obtained for rigid underlaying lattices.

Two phases arrive at equilibrium when their chemical potentials become equal. Here we consider the $NiCoFeCrAl_x$ system as a pseudobinary $(NiCoFeCr)_{1-y}Al_y$ alloy [with

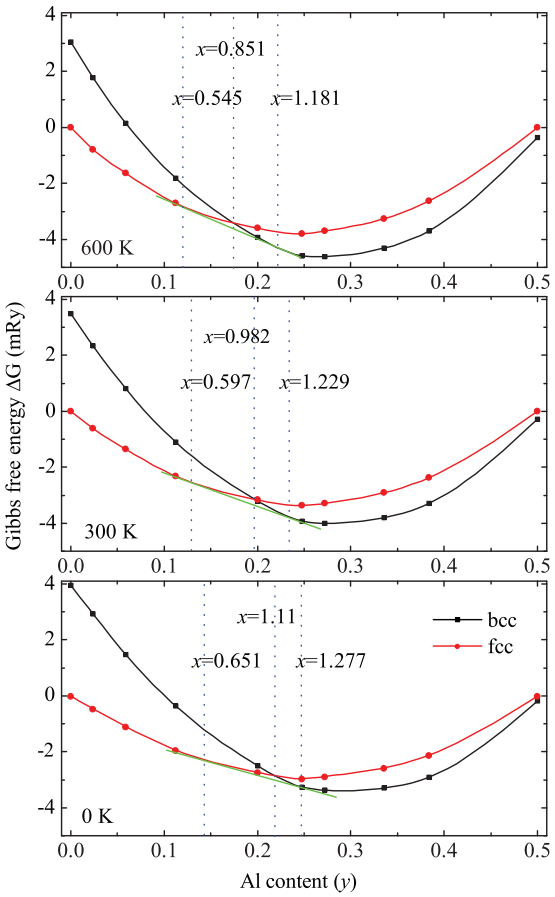

FIG. 2. (Color online) Comparison of the Gibbs free energies for bcc and fcc (NiCoFeCr)$_{1-y}$Al$_y$ ($y = 0.0$–0.5) for $T = 0$,300 and 600 K. Note that $y = x/(4 + x)$, where x is the atomic fraction of Al in NiCoFeCrAl$_x$.

$y = x/(4 + x)$] and compute the relative formation energy according to $\Delta G^{\alpha}(y) = G^{\alpha}(y) - (1 - 2y)G^{\mathrm{fcc}}(0) - 2yG^{\mathrm{fcc}}(0.5)$, where α stands for fcc or bcc, and $G^{\alpha}(y)$ is the Gibbs free energy per atom for (NiCoFeCr)$_{1-y}$Al$_y$ in the α phase. This is approximated as $G^{\alpha}(y) \approx E^{\alpha}(y) - TS_{\mathrm{mix}}(y) - TS^{\alpha}_{\mathrm{mag}}(y)$, where $E^{\alpha}(y)$ is the total energy per atom for (NiCoFeCr)$_{1-y}$Al$_y$ in the α phase, and T is the temperature. The two entropy terms are estimated within the mean-field approximation. Namely, the mixture entropy of ideal solutions is $S_{\mathrm{mix}} = -k_B \sum_{i=1}^{5} c_i \ln c_i$, and the magnetic entropy $S_{\mathrm{mag}} = k_B \sum_{i=1}^{5} c_i \ln(1 + \mu_i)$, where c_i is the concentration and μ_i the magnetic moment of the ith alloying element. Accordingly, all chemical and magnetic short range order effects and the longitudinal spin fluctuations are neglected (i.e., for each alloy composition we assume constant local magnetic moments with temperature). The above phenomenological approximation for the magnetic entropy was previously used to estimate the free energy of paramagnetic Fe[34] and Fe-based alloys[31,35] having noninteger magnetic moments. The present Gibbs free energies at different temperature are plotted in Fig. 2. According to the rule of common tangent line, we find that at room temperature NiCoFeCrAl$_x$ has single fcc phase for $x \lesssim 0.597$ ($y \lesssim 0.130$), single bcc phase for $x \gtrsim 1.229$ ($y \gtrsim 0.235$), and two phases (duplex) between the above limits. In terms of valence electron concentration, the present theory predicts that at 300 K the fcc phase is stable for VEC $\gtrsim 7.57$ and the bcc one for VEC $\lesssim 7.04$. These theoretical solubility limits should be compared to 8.0 and 6.87 estimated by Guo *et al.*[14] and 7.67–7.88 and 7.06–7.29 observed in experiments.[2,10]

The calculated elastic parameters of NiCoFeCrAl$_x$ HEAs' are listed in Table II. We notice that the elastic parameters obtained for the fcc and bcc phases around $x = 1$ are surprisingly close to each other. When considering the fcc or bcc structure separately, it is found that the three cubic elastic constants (c_{ij}) and the polycrystal elastic moduli (B, G, and E) decrease with increasing Al content. However, the Cauchy pressure (c_{12}–c_{44}), the two anisotropy ratios (A_{Z} and A_{VR}), the Poisson's ratio (ν), and the B/G ratio increase with x in the fcc phase.

The somewhat different impact of Al on the elastic parameters of fcc and bcc NiCoFeCrAl leads to local maxima in (c_{12}–c_{44}), ν, and B/G versus x when plotted for fcc for $x \leqslant 1$ and for bcc for $x \geqslant 1$ (Fig. 3). In order to understand these trends, we should see how alloying influences the single-crystal elastic parameters when going from Al-free fcc to bcc NiCoFeCrAl$_2$. As $B(x)$ follows a nearly linear trend, the nonlinearity of c_{11} and c_{12} is due to the particular trend obeyed by the tetragonal shear elastic constant $c' = (c_{11} - c_{12})/2$. This parameter is connected to the curvature of the total energy as a function of the tetragonal lattice parameter c/a at fixed volume.[20] According to the calculated trend of $c'(x)$ (Table II), Al strongly reduces the dynamical stability of the fcc lattice and slightly increases that of the bcc lattice. At the same time, Al stabilizes thermodynamically the bcc structure relative to the fcc one (Figs. 1 and 2). Combining these two effects, we

TABLE II. Theoretical single-crystal elastic constants [c_{ij}, $c' = (c_{11} - c_{12})/2$, $A_{\mathrm{Z}} = c_{44}/c'$], Cauchy pressure ($c_{12}$–$c_{44}$), and polycrystal elastic moduli (B, G, E, ν, A_{VR}, and B/G) for fcc and bcc NiCoFeCrAl$_x$ alloys as a function of Al content. The unit is GPa except for the dimensionless A_{Z}, A_{VR}, ν, and B/G.

x		c_{11}	c_{12}	c_{44}	c'	A_{Z}	(c_{12}–c_{44})	B	G	E	ν	A_{VR}	B/G
0	fcc	271	175	189	48.0	3.94	−14.3	207	110	280	0.275	0.209	1.88
0.3	fcc	246	171	177	37.3	4.75	−6.12	196	96	248	0.289	0.262	2.04
0.5	fcc	233	169	171	32.2	5.29	−2.13	190	89	231	0.297	0.295	2.13
1.0	fcc	214	167	158	23.5	6.85	9.00	183	76	201	0.317	0.369	2.40
1.0	bcc	214	160	152	27.2	6.72	7.84	178	78	204	0.309	0.311	2.29
1.3	bcc	208	151	150	28.1	5.59	0.80	170	78	203	0.301	0.298	2.17
1.5	bcc	205	148	149	28.5	5.34	−1.66	167	78	202	0.297	0.293	2.13
2.0	bcc	197	140	147	28.3	5.26	−6.56	159	77	199	0.291	0.289	2.06

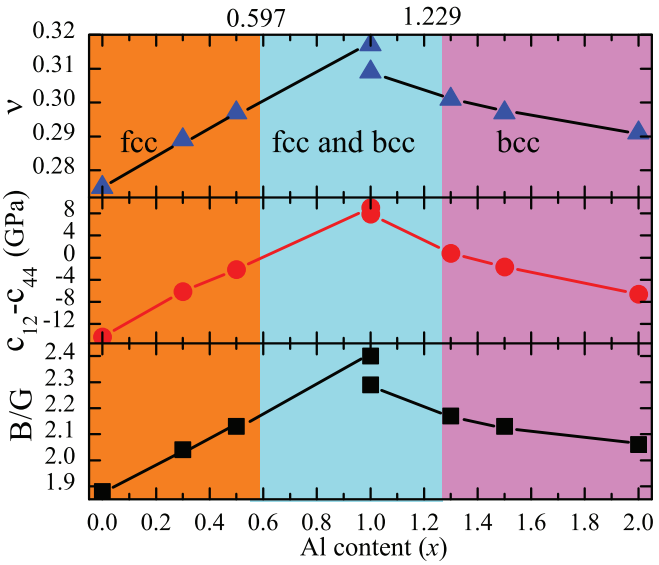

FIG. 3. (Color online) Theoretical Poisson's ratio (upper panel), Cauchy pressure (middle panel), and Pugh ratio (lower panel) for $NiCoFeCrAl_x$ as a function of Al fraction. Results are shown for the fcc phase for $x \leqslant 1$ and for the bcc phase for $x \geqslant 1$. The two single phase regions (fcc or bcc) as well as the two-phase (duplex) region (fcc and bcc) corresponding to Fig. 2 (300 K) are marked by different (colored) areas.

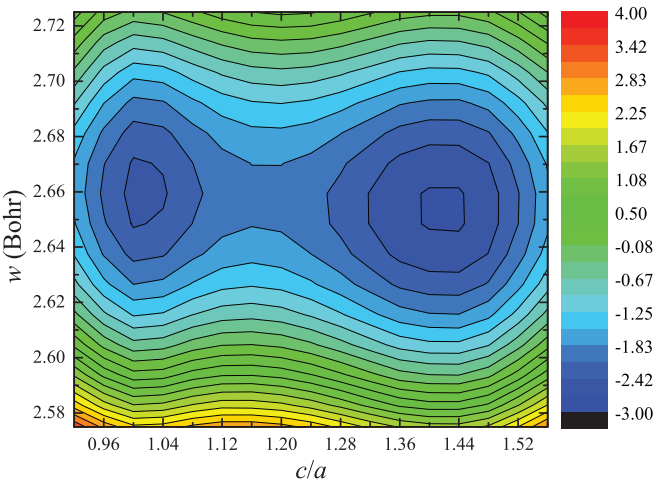

FIG. 4. (Color online) Energy contour (in mRy) for paramagnetic FeCrNiCoAl as a function of the tetragonal ratio (c/a) and the Wigner-Seitz radius (w, in Bohr).

obtain that around the duplex region (Fig. 3) the $NiCoFeCrAl_x$ system has two very similar distinct local minima within the Bain configurational space (described by c/a and volume) with a clear barrier between them (Fig. 4). One local minimum corresponds to the bcc phase ($c/a = 1$) and another to the fcc phase ($c/a = \sqrt{2}$). This situation is rather unusual for elemental cubic transition metals and their alloys,[36] for which the thermodynamically unstable cubic structure is usually also dynamically unstable (or barely stable).

Negative Cauchy pressure has been associated with the covalent nature of the metallic bond and is characteristic to brittle alloys.[37] According to Pugh,[38] materials with a B/G ratio above 1.75 are ductile. For isotropic materials, the Pugh criteria for ductility implies $\nu > 0.26$, which has been confirmed for bulk metallic glasses.[39] In the case of $NiCoFeCrAl_x$, alloys outside of the two phase region possess small or negative Cauchy pressure, and their Pugh and Poisson's ratios are also the lowest (Fig. 3). On the other hand, close to $x = 1$ both phases have large positive Cauchy pressure, and large B/G and ν, indicating strong metallic character and enhanced ductility for these systems.

Based on the above theoretical predictions, we conclude that the paramagnetic $NiCoFeCrAl_x$ HEAs have exceptional micromechanical properties close to or within the duplex region. The disclosed results and developments demonstrate that advanced *ab initio* alloy theory is able treat the newly emerging challenging questions of the HEAs.

Work supported by the Swedish Research Council, the European Research Council, and the China Scholarship Council. The National 973 Project of China (Grant No. 2011CB606401) and the Hungarian Scientific Research Fund (OTKA 84078) are also acknowledged for financial support.

[1] J. W. Yeh, S. K. Chen, S. J. Lin, J. Y. Gan, T. S. Chin, T. T. Shun, C. H. Tsau, and S. Y. Chang, Adv. Eng. Mater. **6**, 299 (2004).
[2] Y. F. Kao, T. J. Chen, S. K. Chen, and J. W. Yeh, J. Alloys Compd. **488**, 57 (2009).
[3] Y. F. Kao, S. K. Chen, T. J. Chen, P. C. Chu, J. W. Yeh, and S. J. Lin, J. Alloys Compd. **509**, 1607 (2011).
[4] H. P. Chou, Y. S. Chang, S. K. Chen, and J. W. Yeh, Mater. Sci. Eng. B **163**, 184 (2009).
[5] Y. J. Zhou, Y. Zhang, Y. L. Wang, and G. L. Chen, Appl. Phys. Lett. **90**, 181904 (2007).
[6] Y. P. Wang, B. S. Li, M. X. Ren, C. Yang, and H. Z. Fu, Mater. Sci. Eng. A **491**, 154 (2008).
[7] T. T. Shun, C. H. Hung, and C. F. Lee, J. Alloys Compd. **493**, 105 (2010).
[8] C. Li, J. C. Li, M. Zhao, and Q. Jiang, J. Alloys Compd. **504S**, S518 (2010).
[9] Y. F. Kao, T. D. Lee, S. K. Chen, and Y. S. Chang, Corrosion Sci. **52**, 1026 (2010).
[10] W. R. Wang, W. L. Wang, S. C. Wang, Y. C. Tsai, C. H. Lai, and J. W. Yeh, Intermetallics **26**, 44 (2012).
[11] S. K. Chen and Y. F. Kao, AIP Adv. **2**, 012111 (2012).
[12] Y. Zhang, S. G. Ma, and J. W. Qiao, Metall. Mater. Trans. A **43**, 2625 (2012).
[13] C. Zhang, F. Zhang, S. L. Chen, and W. S. Cao, JOM **64**, 830 (2012).
[14] S. Guo, C. Ng, J. Lu, and C. T. Liu, J. Appl. Phys. **109**, 103505 (2011).
[15] M. S. Lucas, L. Mauger, J. A. Munoz, Y. M. Xiao, A. O. Sheets, S. L. Semiatin, J. Horwath, and Z. Turgut, J. Appl. Phys. **109**, 07E307 (2011).
[16] B. Cantor, I. T. H. Chang, P. Knight, and A. J. B. Vincent, Mater. Sci. Eng. A **375**, 213 (2004).

[17]Y. J. Zhou, Y. Zhang, F. J. Wang, and G. L. Chen, Appl. Phys. Lett. **92**, 241917 (2008).
[18]P. Hohenberg and W. Kohn, Phys. Rev. **136**, B864 (1964).
[19]O. K. Andersen, O. Jepsen, and G. Krier, in *Lectures on Methods of Electronic Structure Calculation* (World Science, Singapore, 1994), p. 63.
[20]L. Vitos, *The EMTO Method and Applications in Computational Quantum Mechanics for Materials Engineers* (Springer, London, 2007).
[21]L. Vitos, Phys. Rev. B **64**, 014107 (2001).
[22]L. Vitos, H. L. Skriver, B, Johansson, and J. Kollár, Comp. Mater. Sci. **18**, 24 (2000).
[23]B. L. Gyorffy, Phys. Rev. B **5**, 2382 (1972); P. Soven, Phys. Rev. **156**, 809 (1967).
[24]L. Vitos, I. A. Abrikosov, and B. Johansson, Phys. Rev. Lett. **87**, 156401 (2001).
[25]F. Y. Tian, L. K. Varga, N. X. Chen, L. Delczeg, and L. Vitos, Phys. Rev. B **87**, 075144 (2013).
[26]J. P. Perdew, K. Burke, and M. Ernzerhof, Phys. Rev. Lett. **77**, 3865 (1996); **78**, 1396(E) (1997).
[27]P. A. Korzhavyi, A. V. Ruban, I. A. Abrikosov, and H. L. Skriver, Phys. Rev. B **51**, 5773 (1995).
[28]V. L. Moruzzi, J. F. Janak, and K. Schwarz, Phys. Rev. B **37**, 790 (1988).
[29]G. Grimvall, *Thermophysical Properties of Materials* (North-Holland, Amsterdam, 1999).
[30]B. L. Györffy, A. J. Pindor, J. Staunton, G. M. Stocks, and H. Winter, J. Phys. F: Met. Phys. **15**, 1337 (1985); T. Oguchi, K. Terakura, and N. Hamada, *ibid.* **13**, 145 (1983); F. J. Pinski, J. Staunton, B. L. Györffy, D. D. Johnson, and G. M. Stocks, Phys. Rev. Lett. **56**, 2096 (1986); J. Staunton, B. L. Györffy, A. J. Pindor, G. M. Stocks, and H. Winter, J. Magn. Mater. **45**, 15 (1984).
[31]L. Vitos, P. A. Korzhavyi, and B. Johansson, Phys. Rev. Lett. **96**, 117210 (2006).
[32]H. Zhang, B. Johansson, and L. Vitos, Phys. Rev. B **84**, 140411(R) (2011).
[33]D. Music, T. Takahashi, L. Vitos, C. Asker, I. A. Abrikosov, and J. M. Schneider, Appl. Phys. Lett. **91**, 191904 (2007).
[34]G. Grimvall, Phys. Rev. B **39**, 12300 (1989).
[35]L. Vitos, J.-O. Nilsson, and B. Johansson, Acta Mater. **54**, 3821 (2006).
[36]P. Söderlind, O. Eriksson, J. M. Wills, and A. M. Boring, Phys. Rev. B **48**, 5844 (1993).
[37]D. Nguyen-Manh, M. Mrovec, and S. P. Fitzgerald, Mater. Trans. **49**, 2497 (2008).
[38]S. F. Pugh, Philos. Mag. **45**, 823 (1954).
[39]X. J. Gu, A. G. McDermott, S. Joseph Poon, and G. J. Shiflet, Appl. Phys. Lett. **88**, 211905 (2006).